IEEE Access
Multidisciplinary | Rapid Review | Open Access Journal

Received March 4, 2020, accepted April 15, 2020, date of publication April 21, 2020, date of current version May 6, 2020.

*Digital Object Identifier 10.1109/ACCESS.2020.2989240*

# A New Very Long Baseline Interferometry Method Based on the Uplink Signal

**LINSHAN XUE[1], WEIREN WU[2,3], AND XUE LI[4,5]**

[1]School of Mechanical and Electrical Engineering, University of Electronic Science and Technology of China, Chengdu 611731, China
[2]School of Mechanical and Electrical Engineering, University of Electronic Science and Technology of China, Chengdu 611731, China
[3]China's Lunar Exploration & Space Engineering Center, Beijing 100190, China
[4]School of Microelectronics and Communication Engineering, Chongqing University, Chongqing 400044, China
[5]School of Astronautics and Aeronautics, University of Electronic Science and Technology of China, Chengdu 611731, China

Corresponding author: Xue Li (lixue.1981@hotmail.com)

This work was supported by under Grant 060301 and Grant B0110.

**ABSTRACT** Very long baseline interferometry (VLBI) is widely used for astronomical observations and navigation of deep space receivers. To solve the problems of the downlink signal being excessively weak to be received and the excessively large acquisition time, a new VLBI measurement method based on the uplink signal is proposed. Deep space ground stations can provide radio measurement signals for deep space spacecraft via the uplink. The range, Doppler and VLBI can be determined by the spacecraft through signals from multiple ground stations. In this manner, a higher signal to noise ratio (SNR) can be obtained. This study involves the development of a prompt acquisition algorithm for high dynamic deep space signals. Furthermore, the measurement and tracking of the phases of multiple VLBI stations by deep space receiver employing the uplink are analyzed. The use of the algorithms reduce the acquisition time for deep space receiver, and high precision results can be obtained for the VLBI measurement. Compared with the traditional VLBI method, the ranging error on the same distance is effectively improved, and the angle measurement accuracy is better than delta differential one way ranging ($\Delta$DOR). Because multiple spacecraft are not needed, there are fewer limitations than same beam interferometry (SBI).

**INDEX TERMS** Navigation, very long baseline interferometry, acquisition and tracking, interferometry.

## I. INTRODUCTION

Very long baseline interferometry (VLBI) has received considerable attention in the deep space communication domain due to its high resolution with a long baseline. A VLBI system can be used to obtain the distance, Doppler and angle of deep space spacecraft [1]. Through high precision orbit measurement data, the ground stations can precisely define the orbit of the spacecraft and control it effectively. The ground station calculates the distance by measuring the time delay to the spacecraft [2]. The Doppler of the spacecraft is measured considering the carrier phase rate [3], and the measurement of these two parameters can provide high precision information along the line of sight direction. Furthermore, the VLBI system can be used to obtain high precision angle measurement results. Based on these three measurements, the system can determine the precise position of the spacecraft [4].

Specifically, four main ranging methods are widely used. The tone ranging system employs a series of square or sine waves. However, solving the distance ambiguity is a complex and time consuming process [1]. A pseudo noise (PN) ranging system is similar to the global positioning system (GPS), albeit with a longer spread spectrum code period. National Aeronautics and Space Administration (NASA) and the Consultative Committee for Space Data Systems (CCSDS) proposed a ranging composite subcode having a length of 1009470. The acquisition time of the composite pseudocode depends on the acquisition time of the longest subcode [5], [6], [8]. A square wave ranging system relies on a set of square waves, each of which carries a frequency of 2n times to another wave. This method has the advantages of a shorter acquisition time and simpler Doppler compensation. The hybrid ranging method proposed by NASA can be used to extend the distance of ranging from 150000 km (tone ranging) to 644000 km (hybrid ranging). Single tone and PN ranging systems are used to measure the distance, and the ranging accuracy is ensured through the ranging tone [7], [8].

The associate editor coordinating the review of this manuscript and approving it for publication was Jenny Mahoney.


This work is licensed under a Creative Commons Attribution 4.0 License. For more information, see https://creativecommons.org/licenses/by/4.0/

If the system get the ranging results, the local stations can locate the spacecraft as long as the angle information of the spacecraft is obtained by VLBI. The VLBI is similar to traditional interferometer. The interferometer method is widely used in astronomy, medical treatment, navigation and material detecting. There are two main interferometry methods, microwave interferometry and optical interferometry. At present, microwave interferometer is generally used in VLBI, and optical interference station is under construction. Besides, the interferometer can be used in medical treatment and detecting. The digital speckle pattern interferometry (DSPI) method can be used to measure the strain distribution in cortical bone around miniscrew implants [9] and temperature distribution of flames [10]. Reference [11], [12] expand the use of high speed digital holographic interferometer. Reference [13] shows the way of detecting the surface relief and refractive index gratings of chalcogenide glass by interferometer. Wei an provides a method to measure the initial random phase of the speckle pattern, which improves the estimation accuracy of the initial phase [14]. It effectively improves the measurement accuracy of the phase shift by having many phase-shifting steps before the deformation. Microwave interferometer is generally used in VLBI.

In the VLBI measurement, the group delay is obtained by correlating the signals received from two remote observatories. The following four measurement methods are available: differential one way ranging (DOR), ΔDOR, SBI, connected element interferometry (CEI). The DOR measures the phase difference of two sine waves received by two stations from the spacecraft. The correlation processing algorithm can be used to obtain considerably accurate measurement results [1]. The ΔDOR performs the measurement for the radio source and the spacecraft at the same time or alternately and determines the difference between the accurate radio source distance and the spacecraft distance. Compared with the DOR method, the use of this method can reduce the measurement errors arising from sources such as atmospheric perturbations, station location uncertainties, and instrument errors [16], [17]. In recent times, the ESA has gradually adopted the wideband ΔDOR (W−ΔDOR) technology to suppress the thermal noise and phase jitter of the radio source and spacecraft [18]. The SBI can be used to track multiple spacecraft simultaneously. However, the spacecraft needs to be in the same beam coverage of the antenna. The performance of SBI is better than that of the ΔDOR because it calculates the phase difference between stations and spacecraft [20]. The main objective of the CEI is to solve the problem of the baseline being extremely long and the data being unable to be synchronized simultaneously. The approach approximates the performance of a long baseline measurement by measuring multiple short baselines [21].

Table 1 presents a comparison of the performances of different methods [3]. As the location error of the station is extremely large, the DOR measurement is not presented in the Table.

**TABLE 1. Performance comparison of different methods (baseline is approximately 11000km).**

| Measurement item | Measurement accuracy |
|---|---|
| Ranging | 1–5 m |
| Velocity measure | 1 mm/s |
| ΔDOR | X band: 6–15 nrad<br>Ka band: 1 nrad |
| SBI | <1 nrad |
| CEI | 50 nrad |

This paper presents a new VLBI method based on the uplink signal. As the signal is transmitted through the ground deep space station, the SNR is considerably higher than that of the downlink signal. The measurement signal is used to determine the distance, Doppler and angle in the spacecraft. This method involves two advantages: First, the signal power of the ground deep space station is higher than that of the spacecraft by approximately 20 dB. Second, the spacecraft calculates the distance, Doppler and angle values through the uplink and transmits these values to the ground station via the downlink. The measurement results obtained using this method exhibit reduced random errors, and the error of the spacecraft system clock can be corrected effectively.

However, the uplink measurement involves certain challenges, such as in terms of distinguishing multiple ground stations, prompt acquisition of the signal, and stable tracking of the signal. In this work, the paper solve those problems and give the design of new VLBI system. At last, compared with the traditional VLBI method, the ranging error on the same distance is effectively improved, and the angle measurement accuracy is higher than Δ DOR. Because multiple spacecraft are not needed, there are fewer limitations than SBI.

The outline of the remaining paper is as follows. First, the traditional and new VLBI signal models, the transmitting and receiving methods are given in Section II. Section III and section IV presents the acquisition and tracking methods of the novel VLBI method. Besides, the performance of those process is analyzed. The simulations to validate the VLBI measurement performance in Section V. Finally, the conclusions and future work are presented in Section VI.

## II. VLBI MEASUREMENT

This section describes the traditional VLBI technologies and novel VLBI methods. The theory and limitations of the existing techniques are first introduced. Subsequently, the problems that must be overcome using the new methods are discussed, and several solutions are presented.

### A. TRADITIONAL VLBI TECHNOLOGIES

The signal from a deep space spacecraft arrives at two remote deep space telemetry track and command (TT&C) stations on Earth via plane waves. The VLBI station performs the signal amplification, down conversion and filtering. Subsequently, the signal is sampled and time synchronized. The results are

**TABLE 2. Performance of the uplink antenna array (using spatial synthesis technology).**

| | NASA (70 m) | China (35 m) | China (66 m) | Uplink antenna array |
|---|---|---|---|---|
| X band EIRP | 114.6 dBW | 104 dBW (10 kW) | 107 dBW (10 kW) | 117 dBW (10 kW) |
| Ka band EIRP | \ | 111 dBW (50 kW) | 114 dBW (50 kW) | 124 dBW (50 kW) |

stored on the storage device for further processing. Finally, the signals from two VLBI stations are cross correlated to obtain the group delay [22].

The differential group delay $\tau_{21}$ between the stations is used for the angle measurement

$$\tau_{21} = \frac{\mathrm{B} \cdot \mathrm{s}}{c} = \frac{B \cdot \cos\theta}{c} \tag{1}$$

Here, $B$ is the length of the baseline between two VLBI stations, $\mathbf{s}$ is the direction unit vector of the spacecraft, $\theta$ is the angle between the baseline and the direction vector, and $c$ is the speed of light. Equation (1) shows that the accuracy of the VLBI angle measurement depends on the baseline length and accuracy of the differential group delay measurement [23], [24].

The VLBI stations can receive the signal from the deep space spacecraft and record the data locally [25]. In this case, the observation time is extremely large, and the carrier noise ratio ($C/N_0$ ) of the signal is extremely low. B. New VLBI technologies

In this work, the VLBI measurement process is conducted on the deep space spacecraft by uplink signal. For spacecraft, the launch power of spacecraft will not exceed 1 kW. There are a few examples. The transmitted signal power of Pioneer missions is 155 W. And the power of Voyager missions is 470 W [23]. However, for the ground VLBI station, its transmitting power is 10 kW-50 kW (China 35m antenna array) or higher. In this manner, the SNR of the uplink can achieve a gain of more than 13∼25 dB due to the use of the ground transmitting station. The equivalent isotropically radiated power (EIRP) of the deep space station antenna array is shown in Table 2. Red font indicates that the construction of the array is in progress.

However, the new system may cause the following problems:

1) If the frequency division mode is adopted, the carrier phase between multiple stations cannot be synchronized, and the angle measurement accuracy cannot satisfy the requirements.

2) If the time division mode is adopted, the signal needs to be acquired and tracked rapidly. But the time division mode cannot be used to realize long term tracking, thereby leading to the failure of high precision measurement.

3) The mode of the code division is reasonable. However, the deep space receiver requires a large period for the spread spectrum code to solve the distance ambiguity. In this process, the coherent and incoherent integration must be performed simultaneously, which requires a large amount of time. In addition, the speed of the spacecraft itself reaches 16 km/s which increases the acquisition time.

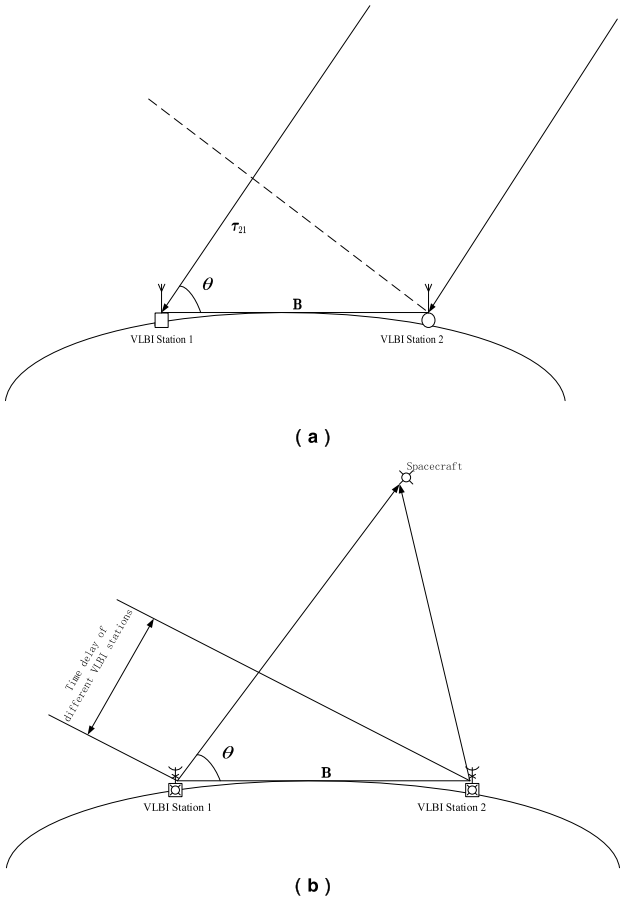


**FIGURE 1. Theory of different VLBI systems. (a)Traditional VLBI.(b)Novel VLBI method.**

Therefore, in this work, the following system is adopted for the measurement. The VLBI station transmits in time, as shown in Fig. 2. The VLBI station switches the transmitted signal by the frequency division plus time division, and the receiver identifies the ownership of the received signal by using a different code. A spread spectrum code that can be used for fast acquisition and tracking is used, as described in Section III. The system also involves a period of idle time when switching to a different frequency, which is used by the receiver to switch the local oscillator to a different frequency.

### *B. THE SYSTEM CAN REALIZE THREE DIFFERENT SWITCHING MODES*

#### 1) SINGLE FREQUENCY TRANSMISSION MODE

This mode, in which only one frequency is provided, is shown in Fig. 2(a). The receiver discriminates the different deep space station signals by using the code division multiplexing access (CDMA). The basic idea of CDMA is to distinguish

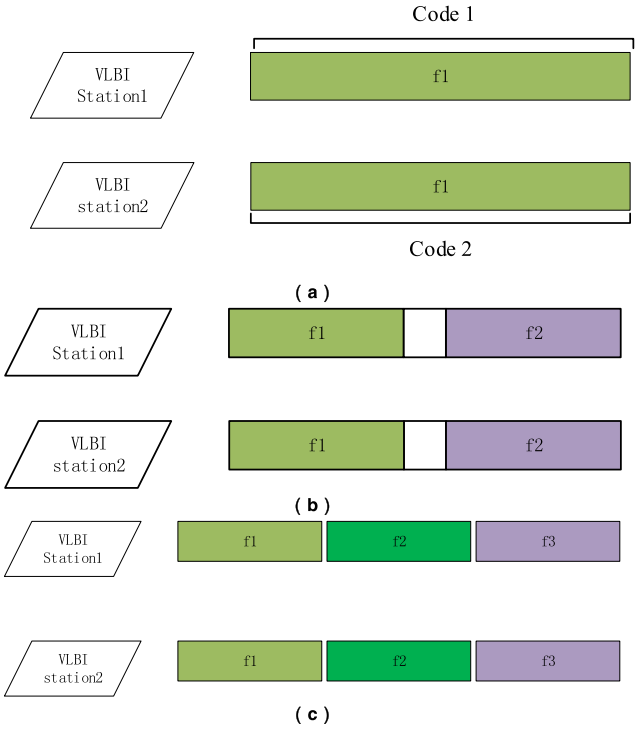


**FIGURE 2.** Switching mode of frequency at the transmitting end of the VLBI station. (a)Signal frequency(b)Dual frequencies (3) Three frequencies.

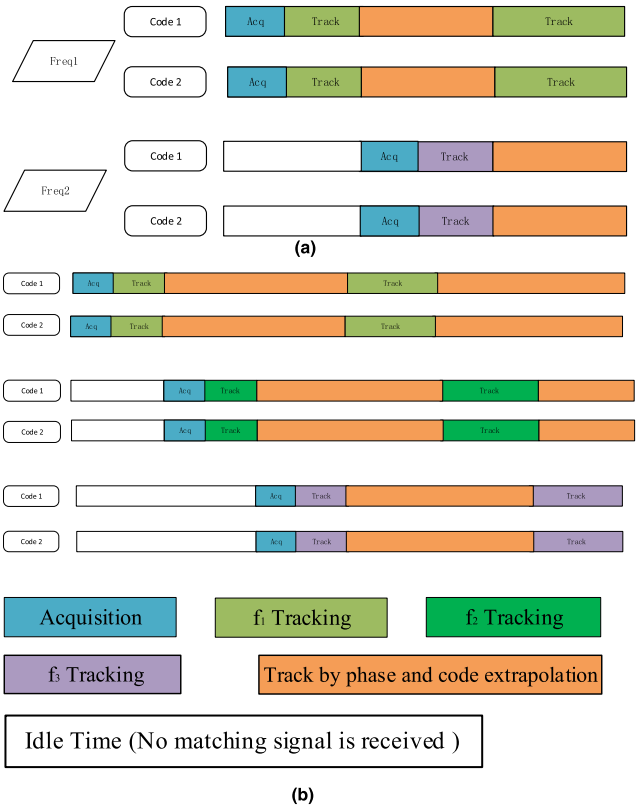


**FIGURE 3.** Frequency switching mode of the spacecraft receiving (a) Dual frequencies (b)Three frequencies.

addresses by different address codes. However, in this case, owing to the presence of only a single frequency, it is impossible to solve the ambiguity of the carrier phase. The accuracy of the angle measurement is extremely low, with a value of only 100 nrad at a baseline length of 3100 km, which cannot satisfy the VLBI requirements. So this paper mainly discusses the following two modes.

#### 2) DUAL FREQUENCY TRANSMISSION MODE

If the spacecraft receives dual frequency signals from two VLBI stations simultaneously, the frequency switching at the transmitting end is as shown in Fig. 2(b). The frequency switching at the receiving end is as shown in Fig. 3(a). The transmission time of each frequency is 0.2 s. In this period, the receiver can complete the acquisition and approximately tracking. Unlike in mode 1, each VLBI station provides two frequencies $f_1\&f_2$ of the signals for tracking. This approach can be used to solve the phase ambiguity and improve the accuracy of the phase measurement.

#### 3) THREE FREQUENCY TRANSMISSION MODE

The three frequency mode is an expansion of the dual frequency mode as shown in Figs.2(c) and 3(b), and it requires more hardware resources to complete the simultaneous acquisition, tracking and extrapolation of the three frequency ($f_1\&f_2\&f_3$) signals. The extrapolation time of each frequency band is larger than that for the dual frequency mode, which leads to additional errors. However, the use of the three frequencies measurement can further improve the accuracy of the carrier phase measurement and reduce the errors in the resolution of the integer ambiguities.

## III. SIGNAL ACQUISITION

In this section, the new signal mode for transmitting and receiving is proposed. It can measure distance without ambiguity in a long distance. The improvement acquisition algorithm for the signal which can acquire Doppler and pseudo code in a short time is discuss. The ranging performance is evaluated by MATLAB.

### A. SNR OF SIGNAL IN THE INTERMEDIATE FREQUENCY (IF)

Deep space communication signals need to be transmitted over a long distance. The free space losses from the Earth to different planets in the solar system are listed in Table 3 [23], [24].

Because the time division system is adopted to transmit the signals, it is necessary for the spacecraft to acquire the signals rapidly. The proposed signal, as per Fig. 2 and Fig 3. is acquired, following the approach outlined in Fig.4.

**TABLE 3. Free space loss from the Earth to planetary bodies in the solar system**

| Planetary body | Farthest distance from the Earth ($10^6$ km) | Free space loss corresponding to the longest distance (dB) (X/Ka) |
|---|---|---|
| Moon | 0.4055 | 222.6616/234.7028 |
| Mercury | 221.9 | 277.4249/289.4661 |
| Venus | 261.0 | 278.8346/290.8758 |
| Mars | 401.3 | 282.5712/294.6124 |
| Jupiter | 968 | 290.2193/302.2605 |
| Saturn | 1659.1 | 294.8993/306.9405 |
| Uranus | 3155.1 | 300.4821/312.5233 |
| Neptune | 4694.1 | 303.9328/315.9740 |

In mode 3, athe VLBI station transmits the signals as described in (2)

$$s_{f_{tri}-VLBI}(t) = \begin{cases} \begin{bmatrix} C_1(t) * D(t) * \cos(2\pi f_1 t) \\ -i * C_2(t) * D(t) * \sin(2\pi f_1 t) \end{bmatrix}, \\ \quad T_h + (n-1)T < t < nT \\ \cos(2\pi f_2 t) - i * \sin(2\pi f_1 t) \\ \quad nT < t < T_h + nT \\ \begin{bmatrix} C_1(t) * D(t) * \cos(2\pi f_2 t) \\ -i * C_2(t) * D(t) * \sin(2\pi f_2 t) \end{bmatrix} \\ \quad T_h + nT < t < (n+1)T \\ \cos(2\pi f_3 t) - i * \sin(2\pi f_3 t) \\ \quad (n+1)T < t < T_h + (n+1)T \\ \begin{bmatrix} C_1(t) * D(t) * \cos(2\pi f_3 t) \\ -i * C_2(t) * D(t) * \sin(2\pi f_3 t) \end{bmatrix} \\ \quad T_h + (n+1)T < t < (n+2)T \\ \cos(2\pi f_1 t) - i * \sin(2\pi f_1 t) \\ \quad (n+2)T < t < T_h + (n+2)T \end{cases} \tag{2}$$

where $s_{f_{tri}-VLBI}(t)$ represents the transmission signal from VLBI station 1. $C_1(t)$ is the CA code with a code length of 1023. $C_2(t)$ is the gold code with a code length of 2047. $D(t)$ is the uplink data that contain the baseline message. $f_i(i = 1, 2, 3)$ represents the radio frequency (RF) frequency. $T_h$ represents the starting time of transmitting the carrier and PN code. $T$ denotes the frequency switching period. For modes 2 and 3 and other VLBI stations, the situation is similar to that expressed in the (2) and is thus not discussed herein.

After the signal is down converted to the IF, the acquisition process is divided into two steps: carrier acquisition and code acquisition as shown in Fig. 4(b). Compared with parallel acquisition in time domain, the acquisition algorithm does not need the Doppler searching process. The signal of the method transmits pure carrier signal at first, and then transmit spread spectrum code signal and data code information. Therefore, the acquisition algorithm of the paper completes the fast fourier transform (FFT) for pure carrier signal at first. In this manner, the Doppler of the signal can be obtained in this process. Then, the algorithm accomplishes the FFT and inverse fast fourier transform (IFFT) for code and carrier signal.

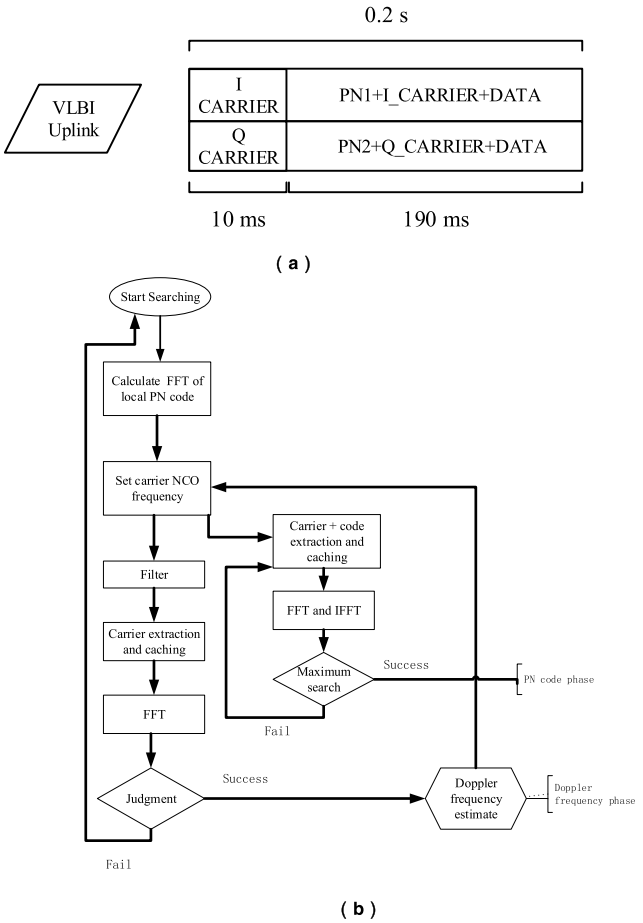


**FIGURE 4.** (a) Modulation mode (b) Carrier and code acquisition.

In the case of large Doppler, the search time of Doppler frequency is excessively reduced.

### 1) CARRIER ACQUISITION

1. The logic control unit uses the local carrier NCO offset $f_{d\_c}$ for the Doppler compensation. Here, $f_{d\_c}$ can be assigned an approximate value considering the orbit of the spacecraft. In general, the compensated residual of the Doppler is less than 250 kHz. The carrier NCO generates the in phase and orthogonal carrier signals based on the frequency tuning word and mixes them with the input signals to the IF (44.96 MHz). The sampling rate is 306 MHz;

2. A 6 order infinite impulse response (IIR) filter is used for the lowpass filtering of the IF signal, and the filtering bandwidth is less than 1.5 MHz. The filtered signal is decimated 102 times, and data for 4 ms are cached for the acquisition of the FFT. The data for 4 ms involve a total of 12000 points, and the data are supplemented to $2^{14}$ points by performing zero filling before the FFT.

3. The sinc interpolation method is used to estimate the FFT results accurately to accurately estimate the carrier frequency.

**TABLE 4. Hardware acquisition time.**

| Process | Clock cycles |
|---|---|
| Carrier cache | 1224000 |
| Carrier FFT | 16384 |
| Max search | 16384 |
| Carrier acquisition total | 1256768 |
| Code cache | 612000 |
| Code FFT | 8192 |
| Complex multiplication | 8192 |
| Code IFFT | 8192 |
| Max search | 8192 |
| Code acquisition total | 644768 |

### 2) CODE ACQUISITION

1. Obtain the accurate estimation for the carrier frequency, adjust the frequency of the input data and obtain the accurate IF signal. The spread spectrum code is used as a composite code, composed of the gold sequence and the CA code. The chip rate is set as 1023 (PN1) and 2047 (PN2), and the chip clock is 1.023 MHz. The acquisition time for the composite PN code is the highest when a single subcode is captured separately and multiple subcodes are captured in parallel.

2. Cache the IF data for 2 ms and decimate the data 102 times. Cache 6000 data points at a sampling rate of 306 MHz. Make up the cached data by zero to $2^{13}$ and FFT.

As shown in Table 4, the carrier acquisition process needs 4.1 ms, and the code acquisition process needs 2.1 ms to be completed. According to the calculated velocity of 16 km/s, the position deviation caused by each acquisition time is not more than 36 m. The distance represented by each code chip is 293 m [26], [27]. The duration of the time division signal is sufficient to complete the acquisition of the carrier and code.

The loss caused by the incomplete chip synchronization is

$$L_{chip} = 20\lg[R(\Delta\tau)] = 20\lg(1 - |\Delta\tau|) \tag{3}$$

When the chip value of the incomplete synchronization is 1/4, the loss is $L_{chip} = -2.5dB$ [28]. The SNR before detection ($SNR_{BD}$) is

$$S/N_{bd} = (C/N_0)_{IF} - 10\lg(\frac{1}{T}) - L_{chip} \tag{4}$$

$(C/N_0)_{IF}$ is the $C/N_0$ of the received signal for the antenna end. T is the coherent integration time, which is set as 2 ms.

Table 2 indicates that the existing transmitting EIRP of the ground VLBI station is 107 dBW. For instance, the X band antenna gain of the Voyager spacecraft is 48 dB, and the beam width is 0.5° [23]. Considering the farthest distance between Neptune and the Earth as an example, the X band uplink signal attenuation is 303 dB. The IF signal power received by the spacecraft is −148 dBW, which means that $C/N_0$ is 52 dB-Hz (calculated considering the thermal noise power spectrum as −204 dBW/Hz). Considering the complexity of the deep space electromagnetic environment, $C/N_0$ is set as 43 dB-Hz (−20 dB) for the simulation in this work. The $SNR_{BD}$ can be calculated as 13.5 dB.

Next, the detection probability under the $SNR_{BD}$ is calculated. Assuming that the signal in the In-phase (I) and Quadrature (Q) channels exhibits a Gaussian distribution, the envelope of the input signal is $I^2+Q^2$. In the case of single detection, the envelope probability density functions obey the exponential distribution with the mean value obtained using (5) corresponds to zero in the event of no signal.

$$P_n(z) = \frac{1}{2\sigma^2} e^{\frac{-z}{2\sigma^2}} \tag{5}$$

When a signal is received, the envelope probability density functions obey the noncentral distribution of $\chi^2$, as obtained using (6)

$$P_s(z) = \frac{1}{2\sigma^2} e^{\left(-\frac{z+A^2}{2\sigma^2}\right)} I_0\left(\frac{A\sqrt{z}}{\sigma^2}\right) \tag{6}$$

In (5) and (6), $z$ is a random variable, $\sigma^2$ is the noise variance, and A is the signal amplitude. In other words, $A/2\sigma^2$ is the power ratio of the predetected signal to the noise signal. $I_0(\cdot)$ is the Bessel function with zero order.

The paper set the detection threshold as $V_T$. Next, the false alarm probability and detection probability of a single detection can be expressed as $P_{fd}$ and $P_d$, respectively.

$$P_{fd} = \int_{V_T}^{+\infty} P_n(z)dz = e^{-\frac{v_T}{2\sigma^2}} \tag{7}$$

$$P_d = \int_{V_T}^{+\infty} P_s(z)dz \tag{8}$$

The constant false-alarm rate (CFAR) detection method is used [29]. Therefore, (7) can be modified as

$$V_T = -2\sigma^2 In(P_{fa}) \tag{9}$$

If the system requires a false alarm probability of $10^{-6}$, will be 27.6310. Equation (8) indicates that when the $SNR_{BD}$ before detection is 13.5 dB, the single detection probability is more than 0.9.

Subsequently, 1000 simulations were conducted to simulate the single detection probability, which yields the limit SNR at the IF of the system. The simulation result as shown in Fig. 5.

The CA codes can be used to measure distances of 299792m and 599878 m without ambiguity, respectively. However, the deep space detection range is several or even dozens of astronomical units (AU). If the two PN codes are used separately, the cycle ambiguity of the pseudocode may be generated. If the calculation error of the cycle ambiguity is more than 1, ranging integer ambiguity may be generated.

Consequently, after acquiring the two PN codes, due to the mutual quality of the length of the two pseudocodes, the cycle ambiguity of the PN codes can be resolved using the following methods. The lowest common multiple of the code periods 1023 and 2047 is 2094081. If the code rate is 1.023 MHz, the maximum unambiguity distance is 613675161 m, which can satisfy the requirements of deep space exploration. Specifically, the following methods can be used to solve the ambiguity:

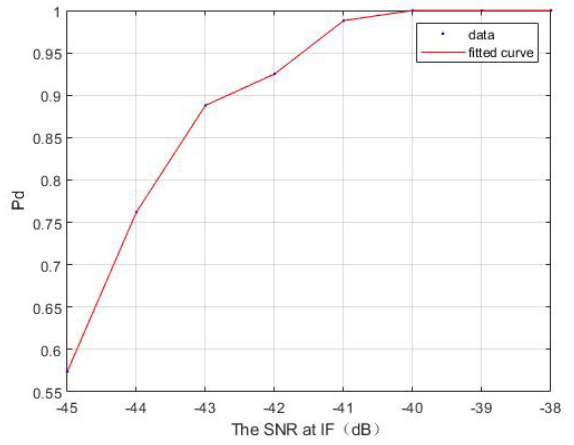


( a )

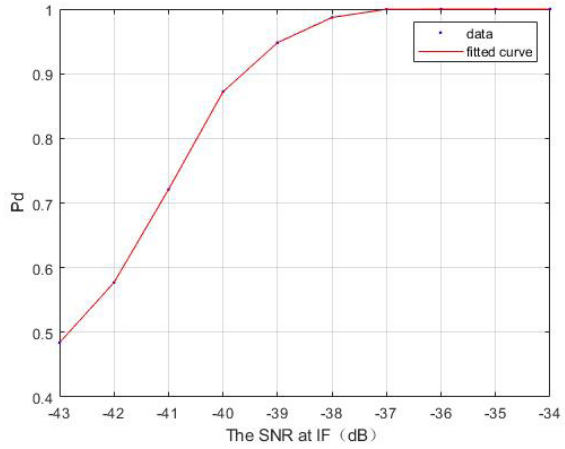


( b )

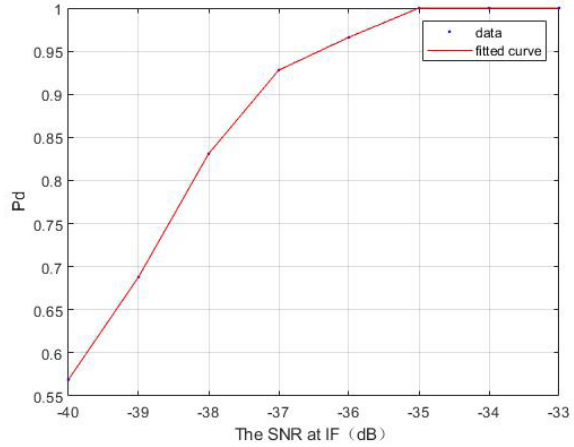


(c)

**FIGURE 5.** Relationship between detection probability Pd and SNR (IF) of the input signal in 1000 simulations: (a) Single carrier (b) CA code with code length of 1023; (c) Gold code with code length of 2047.

The paper uses the Chinese remainder theorem to solve the integer ambiguity. Because the arrival distances of the two codes of the I/Q channels are equal, it can be assumed that the integer ambiguities of one pseudocode is an integer. Subsequently, all the solutions in the solution space of the integer ambiguities can be traversed. Finally, the integer ambiguities of the other code can be obtained. When the solution of the integer ambiguities of one PN code is correct, the difference between the integer ambiguities of the other PN code and the integer closest to it must be minimized as (10).

$$(N_1 + \xi_1/2047) * d_1 \approx (N_2 + \xi_2/1023) * d_2 \qquad (10)$$

where $d_1 = 299792.458m$ and $d_1 = 599877.968m$ are the distances corresponding to the gold code with a code period of 2047 and the CA code with a code period of 1023, respectively. $N_1$ is an integer within 1–1023, and $N_2$ is the integer within 1–2047.

**TABLE 5.** Results of the ranging after acquisition.

| Distance ( m ) | Acquisition Result ( m ) |
|---|---|
| 1000 | 1172 |
| 10000 | 10250 |
| 100000 | 100220 |
| 1000000 | 1000187 |
| 10000000 | 10000115 |
| 100000000 | 100000272 |
| 300000000 | 300000232 |
| 600000000 | 600000171 |

Table 5 presents the ranging results after acquisition, and it can be seen that the ranging error is in a chip.

## IV. SIGNAL TRACKING

This part provides the tracking algorithm. Through inertial navigation system (INS) and orbit extrapolation, the input signal is simulated when there is no matching signal input. Therefore, the tracking loop can achieve the stable tracking of the signal. Finally, the paper gives the measurement accuracy under this algorithm.

### A. EXTRAPOLATION OF CARRIER TRACKING LOOP AND CODE TRACKING LOOP

In the tracking process, the ranging accuracy is further improved [30]. However, if the transmission signal of the VLBI station corresponds to the time division, the tracking lock may be lost in the process of signal switching. To ensure a stable tracking, in this work, the extrapolation mode of the carrier phase and PN code phase is used to lock the tracking loop. The extrapolation process consists of the following five steps, in which $t_1$ is considered as a reference time for the ranging/velocity measurement:

1. Calculate the acceleration considering the spacecraft orbit elements (or spacecraft INS). The radial acceleration value $a(t)$ between the spacecraft and the Earth is calculated by projecting the vector to the Earth;

2. Calculate the velocity $v(t_2)$ of the spacecraft by considering the radial acceleration value $a(t)$ between the spacecraft

and the Earth as follows:

$$v(t_2) = v(t_1) + \int_{t_1}^{t_2} a(t)dt \tag{11}$$

3. The Doppler frequency is calculated using the velocity. This value is introduced to the carrier tracking loop to modify the carrier phase of the generated signal;

4. The calculated value $v(t_2)$ of the radial velocity between the Earth and the spacecraft is used, and the modified pseudo range value $\rho(t_2)$ of the spacecraft is calculated via integration:

$$\rho(t_2) = \rho(t_1) + \int_{t_1}^{t_2} \left[ v(t_1) + \int_{t_1}^{t_2} a(t)dt \right] dt \tag{12}$$

The second term in the right hand side of the (15) is the pseudo distance modifier;

5. The modified pseudo range value is used to calculate the pseudo code phase, which is sent to the code tracking channel for pseudo code phase correction.

Subsequently, the error caused by the extrapolation is analyzed: The switching period of the VLBI station is $T_{SW}$ ($T_{SW} = 0.1s$), the measurement error of the acceleration value $a(t)$ is $\Delta a$, and the measurement error of the velocity is $\Delta v$. The calculation results show that the residual error of the velocity correction is $\Delta a \times T_{SW}$, and the residual error of the pseudo distance correction is $(\Delta v + \Delta a \times T_{SW}) \times T_{SW}$. If the measurement error of the radial acceleration $\Delta a$ between the spacecraft and the Earth is fixed in the switching period $T_{SW}$, the correction residual for the carrier phase and pseudo code phase can be obtained. For example, if $\Delta v \leq 5cm/s$ an $\Delta a \leq 1 \times 10^{-6} g$ when $T_{SW} = 0.2s$, the pseudo range correction residual is $\leq 0.01$ m. Considering the presence of clock errors and other factors, the corrected residual error is expected to be larger. Therefore, in each switching time, the tracking loop needs to relock the signal in an extremely small time.

Consequently, the second order frequency locked loop (FLL) and third order phase locked loop (PLL) are used, which can manage the carrier tracking in various situations. Furthermore, the carrier tracking loop provides a Doppler frequency tuning word to eliminate the Doppler of the code tracking loop [30], [31]. The calculation formula is

$$(f_{code} \times f_d / f_{RF}) \times 2^N / f_s \tag{13}$$

where $f_{code}$ is the PN code frequency, $f_d$ is the Doppler frequency, and $f_{RF}$ is the RF. N is N-bit phase accumulator. $f_s$ is the sampling frequency of the baseband. The frequency tuning word can control the frequency of direct digital synthesizer (DDS). By adding (13) into DDS of PN code, it eliminates the influence of Doppler on the code frequency. In this manner, the second order code tracking loop can be used for the code tracking.

### B. TRACKING LOOP SIMULATION

To simulate the complex environment in deep space, it is assumed that a sinusoidal Doppler rate of approximately 250 Hz is added to the signal with a stable Doppler frequency of more than 50 kHz. The function can be derived and integrated in all the domains, which makes it suitable for simulating the Doppler acceleration change constrained by the orbit. The result of tracking loop when SNR= −20dB as shown in Fig. 6.

It can be seen that in many cases, the use of the tracking loop can yield satisfactory results. The Doppler frequency error does not exceed 5 Hz in the case in which the carrier tracking does not exhibit any deviation in the phase and code extrapolation. If the signal exhibits a deviation in the orbit extrapolation, and the random deviation between the signal and carrier phase within 5 m every 0.5 s is considered, the tracking loop results are as shown in the Figs. 6 and 7. According to the simulation results shown in Figs. 6 and 7, when the phase and code extrapolation errors are small, the loop can track stably. When the orbit extrapolation error occurs, that is, the carrier phase and the code phase are offset at the time of each frequency switching (0.2 s), the loop can be locked again in each switching time.

The Fig.7(a) shows the doppler frequency comparison between the tracking result and the received signal. The sudden change noted in Figs. 7(b) and 7(c) corresponds to the loss of the locking in the FLL and code loop. In this process, the ranging error is less than or equal to 1 m, ignoring the deviation in the tracking results. The Doppler measurement error is less than or equal to 5 Hz in stable tracking. In other words, the speed measurement error in the X band is less than or equal to 0.1875 m/s. Furthermore, the speed measurement error in the Ka band is less than or equal to 0.046875 m/s. On average, the error is smaller than 0.004 m/s in the X band and 9.9562e-04 m/s in the Ka band).

At the same distance, this method can provide higher SNR (approximately 20 dB) to the receiver. Taking the distance between the earth and Neptune as an example, the SNR of the receiver is approximately −130 dBm by the proposed method, while that of the traditional method is −151 dBm. The comparison of random errors over the same distance is shown in the Fig.8. The simulation framework of receiver is shown in APPENDIX.

## V. VLBI MEASUREMENT

In this section, the angle information of the spacecraft is measured by novel VLBI method. Through the tracking results of the section IV, the phase difference can be obtained. And the section V has solved the integer ambiguity. The measurement accuracy is better than most of the current VLBI method, and fewer limitations than SBI.

### A. DUAL FREQUENCY VLBI MEASUREMENT

As described in Section IV, the precision of the PN code ranging is approximately 1 m. This paper take the distance between two VLBI stations is 3100 km as an example. According to (1), the angle measurement accuracy is approximately 3.2e-7 rad. For the VLBI observations, this error is considerably large. Therefore, the system must implement

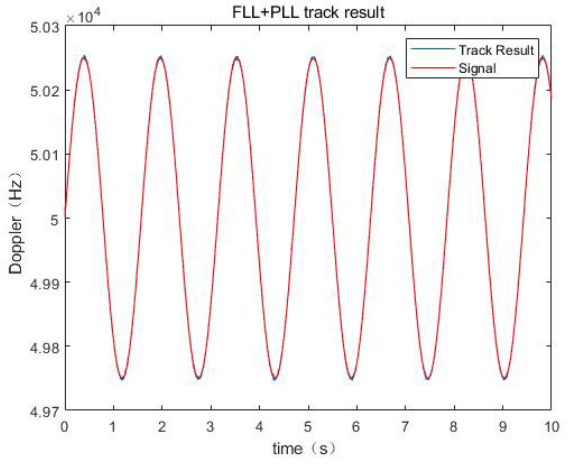


( a )

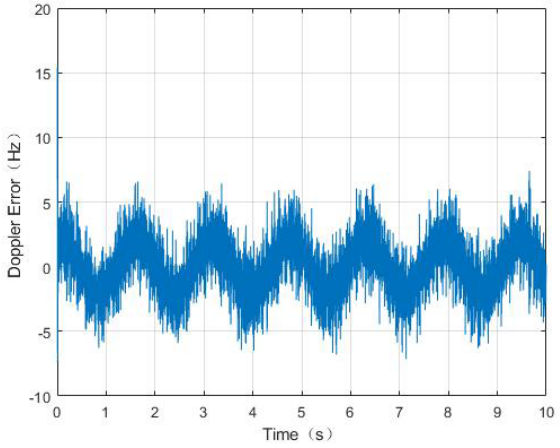


( b )

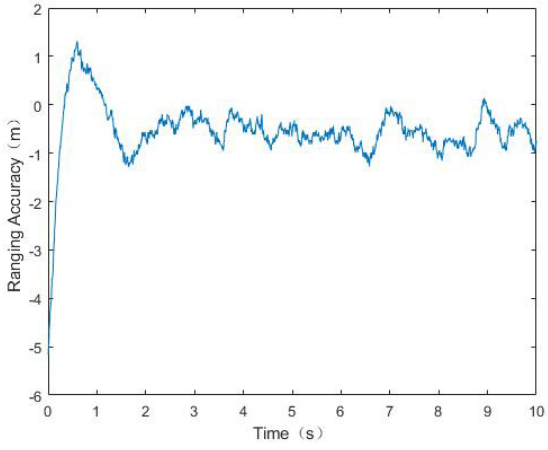


( c )

**FIGURE 6.** Result of the tracking loop at the SNR at IF is −20 dB: (a) Doppler frequency; (b) Doppler error between the tracking result and received signal; (c) Ranging error.

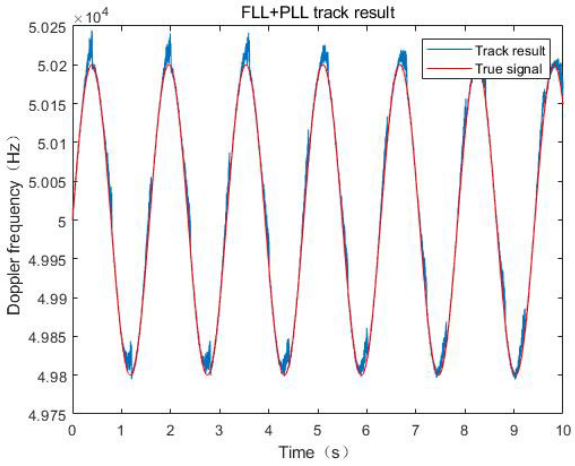


(a)

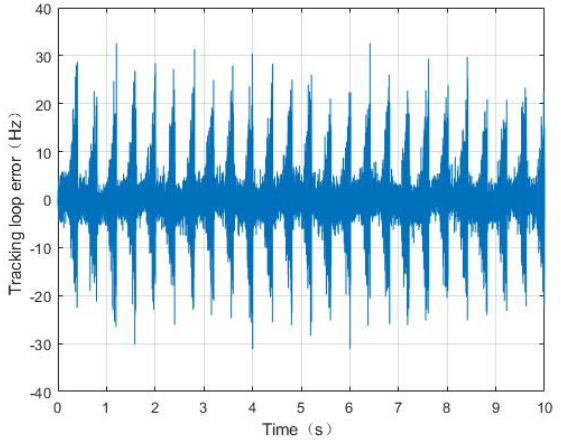


(b)

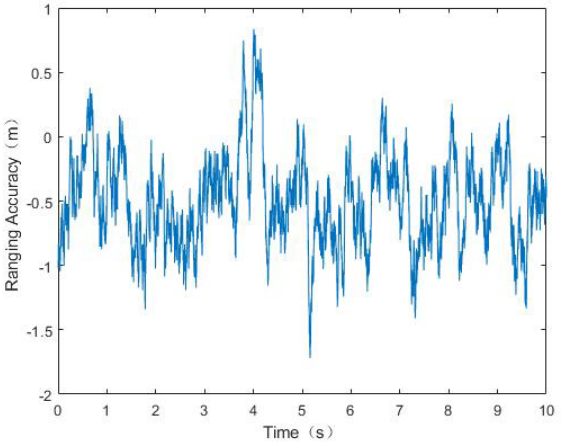


(c)

**FIGURE 7.** Results of tracking loop at the SNR for an IF of −20 dB (complex environment): (a) Doppler frequency;(b) Doppler. error between the tracking result and received signal; (c) Ranging accuracy.

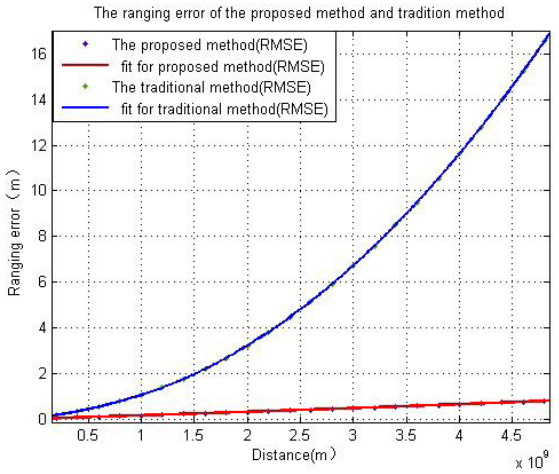


**FIGURE 8.** Random errors at the same distance.

the carrier phase measurement to improve the measurement accuracy of the delay [20].

A synthetic improvement of the algorithm performed based on an existing study [32], [33]. By expanding the algorithm of a short baseline (less than 10 m) to a very long baseline (3100 km), the following methods are adopted to eliminate the carrier ambiguity. First, most of the integer ambiguity is eliminated by employing the PN code measurement results. Next, because the delay difference in the dual frequency signals of the two VLBI stations is the same [34], [35], the integer cycle of the carrier can be searched using the pseudo code technique. The main steps are as follows:

1. The delay difference between VLBI stations 1 and 2 is obtained and converted to a distance difference. The distance measured using the carrier phase is approximately equal to the distance measured using the PN code plus the pseudo code measurement error, as described in (14):

$$\begin{aligned}\rho_{21}^{*} - \Delta\rho \le N_1\lambda_1 + \varphi_{21f1}\lambda_1/2\pi \\ \approx N_2\lambda_2 + \varphi_{21f2}\lambda_2/2\pi \le \rho_{21} + \Delta\rho \end{aligned} \quad (14)$$

Here, $\rho_{21}^{*}$ is the PN code ranging result, $\Delta\rho$ is the ranging error for the PN code, $N_1$ represents the number of cycles of $f_1$, and $\varphi_{21f1}$ is the phase difference for the VLBI station, which is less than one cycle at $f_1$. $\lambda_1$ is the wavelength of $f_1$, and $N_2$, $\varphi_{21f2}$, and $\lambda_2$ are the parameters of $f_2$.

2. Equation 17 is converted to (18).

$$N_1\lambda_1 - N_2\lambda_2 \approx \varphi_{21f2} * \lambda_2/2\pi - \varphi_{21f1}\lambda_1/2\pi \quad (15)$$

Here, the right side of the (15) can be determined using the carrier tracking loop of $f_1$ and $f_2$, and the measurement error is less than one quarter wavelength.

$N_1$ and $N_2$ are searched at $\left[\rho_{21}^{*} - \Delta\rho, \rho_{21}^{*} + \Delta\rho\right]$ to minimize the difference between the left and right sides of the (15). The process flow of the carrier phase measurement is shown in Fig. 9(a).

The parameters are set as follows: If $\Delta\rho \le 2m$, $f_1 = 8GHz$ and $f_2 = 8.1GHz$. While neglecting the error of the

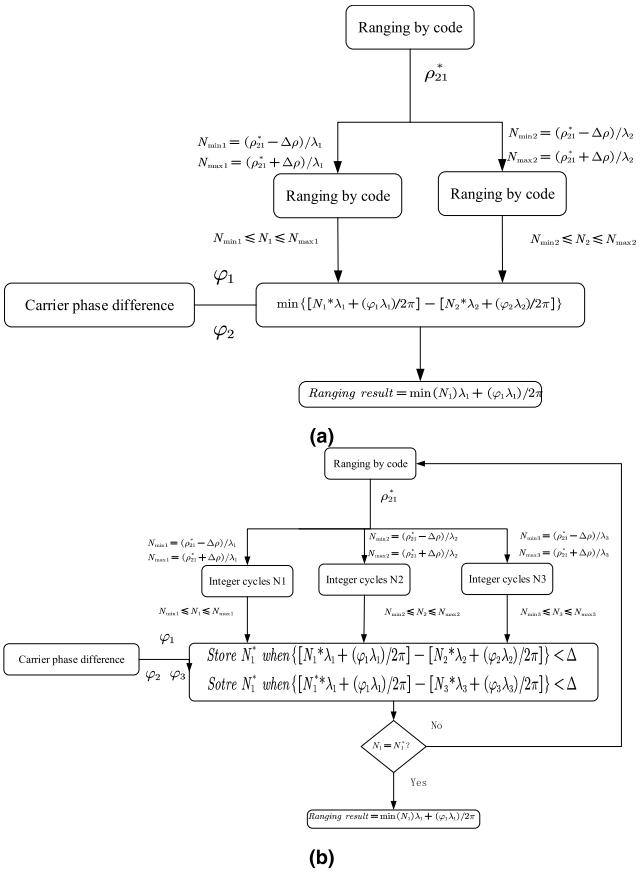


**FIGURE 9.** Process flow of carrier phase measurement: (a) Dual frequency; (b) Three frequencies.

**TABLE 6.** Carrier phase difference at different SNR values.

| SNR at IF(dB) | RMSE of carrier phase difference measurement accuracy (m) | |
|---|---|---|
| | X band (8 GHz) | Ka band (32 GHz) |
| -10 | 6.3020e-05 | 6.5063e-06 |
| -20 | 8.8742e-05 | 1.6614e-05 |
| -30 | 2.1921e-04 | 5.2322e-05 |
| -35 | 3.7648e-04 | 9.8628e-05 |

atmospheric current layer, the measurement accuracy for the carrier phase difference is 1e-3 m. The accuracies at different SNR values are presented in Table 6. The results for the carrier phase ranging are presented in Table 7.

The ranging error is converted to the VLBI measurement error by dividing the ranging error by the baseline length, as in (1). It can be seen that in the range of $\Delta\rho \le 2m$, the result of the ambiguity resolution is correct, and the error is not more than one cycle. When the range is expanded, the result involves a larger error. The RMSE is approximately 1 cm or less, and it is mainly determined by the SNR. When $\Delta\rho \ge 3m$, integer errors may be generated.

### B. THREE FREQUENCY VLBI MEASUREMENT

In the three frequency VLBI measurement, the signal expressed in (2) and Fig. 3(b) is employed. After the three

**TABLE 7.** Result of the ranging according to the carrier phase.

| SNR at IF(dB) | RMSE of ranging result error ( m ) | |
|---|---|---|
| | $\Delta\rho = 1m$ | $\Delta\rho = 2m$ |
| -10 | 1.8164e-05 | 1.8302e-05 |
| -20 | 2.5412e-05 | 2.5640e-05 |
| -30 | 0.0155 | 0.0154 |
| -35 | 0.0190 | 0.0190 |

**TABLE 8.** Result of the ranging considering the carrier phase.

| SNR at IF (dB) | RMSE of the ranging result error when $\Delta\rho \leq 10m$ ( m ) | |
|---|---|---|
| | X band | Ka band |
| -10 | 1.8232e-05 | 1.8606e-06 |
| -20 | 2.5952e-05 | 0.0031 |
| -30 | 0.0140 | 0.0054 |
| -35 | 0.0381 | 0.0106 |

frequency signals are stably tracked, the phase value in the carrier tracking loop is recorded, and the difference is determined [36]. The difference between frequencies 1 and 2 is larger than that between frequencies 2 and 3. In the simulation, $f_3 - f_2$ is one-tenth of $f_2 - f_1$.

The difference between the two methods is as follows:

1. In the process of searching the minimum phase difference, not only is the minimum difference stored, but the values less than a certain threshold are also stored as $N_1^*$;

2. The minimum value for the difference vector in $N_1^*$ and $N_3$ is determined.

Consequently, the robustness of the system is effectively improved. The diagram of the search algorithm is shown in Fig. 9(b). By introducing the carrier phase value of the third frequency, the allowable range of the PN ranging error can be expanded.

The results of the carrier phase ranging are as follows. Since the three frequencies searching can be used to better eliminate the integer ambiguity, a higher carrier frequency is adopted. The parameters are set as follows: $f_1 = 8GHz, f_2 = 8.1GHz, f_3 = 8.11GHz$ denote the X band frequencies, and $f_1 = 32GHz, f_2 = 32.1GHz, f_3 = 32.11GHz$ denote the Ka band frequencies. When $\Delta\rho \leq 10m$, the result of the integer ambiguity resolution is the same as that in Table 8.

The use of the three frequencies searching can improve the search range, which leads to a better robustness and can deal with a larger pseudo code measurement error. However, as the Ka band contains more integer cycles than the X band, the integer cycle estimation error of the Ka band is larger than that for the X band. Nevertheless, the error performance is still better than that of the X band at a low SNR and high SNR.

If the baseline is selected as $B = 3100km$, the angle accuracy can be determined using (1) as higher than 3 nrad.

The ionospheric error is reduced by the difference of dual frequency or triple frequency. If dual frequency signal $f_1 \& f_2$

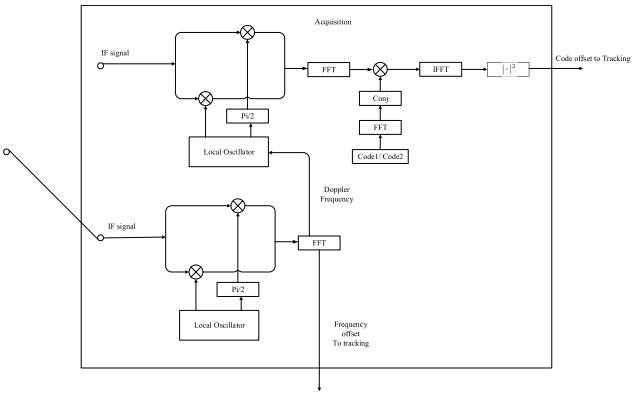


**FIGURE 10.** Tracking process of the paper.

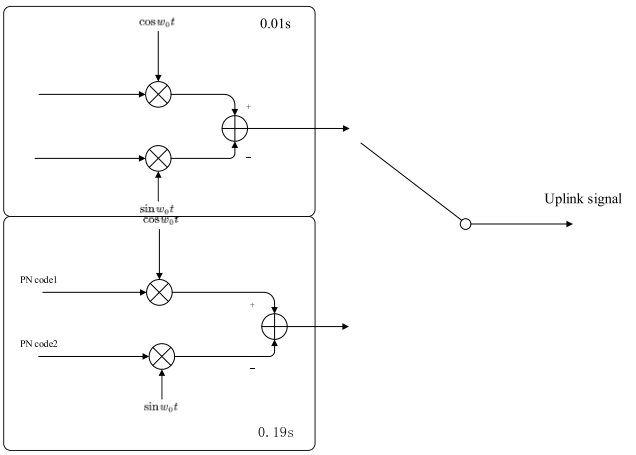


**FIGURE 11.** The acquisition method of the paper.

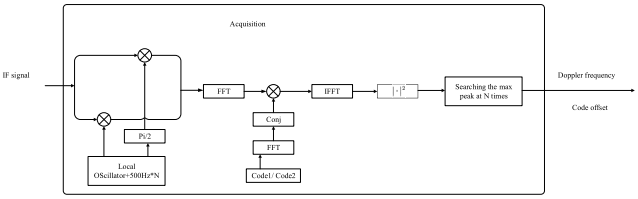


**FIGURE 12.** The transmitting signal.

is used for transmission, and the second order and above items of ionospheric delay are ignored. The delay caused by the ionosphere is

$$\Delta\tau_i = \frac{40.28}{f_i^2}\int N_e(s)ds = \frac{40.28}{f_i^2 \cdot c}TEC \tag{16}$$

where $N_e$ is ionospheric electron density. TEC is the total electron content on the integration path [24]. Time difference between two frequency signals arriving at spacecraft is

$$\Delta t = \Delta\tau_2 - \Delta\tau_1 = \frac{40.28}{f_2^2 \cdot c}TEC - \frac{40.28}{f_1^2 \cdot c}TEC \tag{17}$$

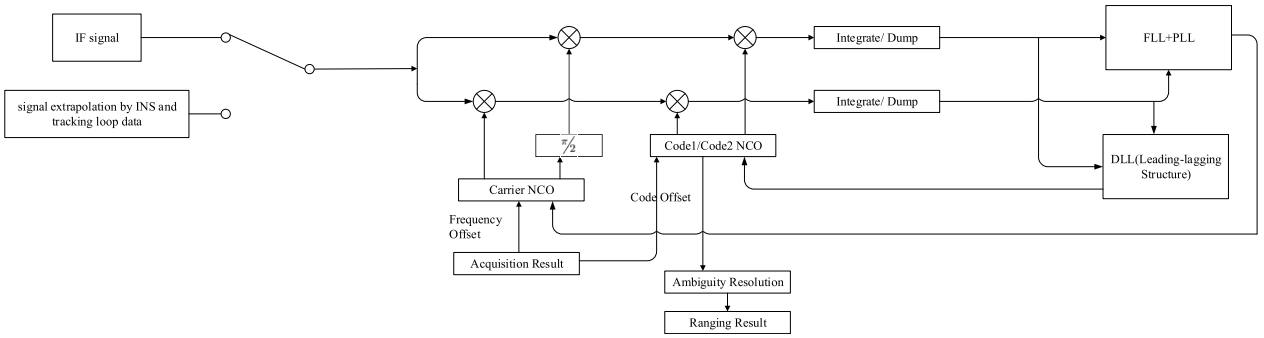


**FIGURE 13.** The parallel acquisition in time domain.

The time delay caused by the ionosphere of two frequency signals can be shown as (18)(19)

$$\Delta\tau_1 = \frac{f_2^2}{f_1^2 - f_2^2}\Delta t \tag{18}$$

$$\Delta\tau_2 = \frac{f_1^2}{f_1^2 - f_2^2}\Delta t \tag{19}$$

As long as the arriving time difference between two signals of different frequencies is measured accurately, the ionospheric delay correction of these two signals can be calculated accurately. According to the data given in the [37], the ionospheric measurement error of current S/X band VLBI stations is approximately 1 mm.

The tropospheric delay models include Hopfield model and Black model etc. The validity of the tropospheric delay model is 92%∼95%. And the current tropospheric delay can also be calibrated by GPS real-time observation. The validity of the tropospheric delay model is approximately 4 mm [38]. So, when SNR is −20 dB, the angle measurement error of X band is 1.61 nrad.

## VI. CONCLUSION AND FUTURE WORK

In this work, the uplink measurement technology for deep space spacecraft is investigated. The modified method can be used for ranging and VLBI measurement at the spacecraft end. This approach resolves the problem of the low SNR of deep space TT&C. Furthermore, the spacecraft ranging and VLBI measurement results are transmitted to the ground through the downlink to enable two way time synchronization. The uplink signals are distinguished via time division. Considering this aspect, a fast acquisition algorithm for the deep space receiver is designed. The theoretical and simulation results show that the acquisition algorithm can achieve long distance and unambiguity acquisition under the condition of a low SNR. The corresponding hardware operation time is calculated, and the algorithm is noted to acquire the signal in a short time.

Subsequently, through the extrapolation of the code phase and carrier phase, stable tracking for the time division signal is conducted. The simulation results show that the loop can be tracked stably when the extrapolation is error free, and it can be locked rapidly in the case of erroneous extrapolation.

Finally, the traditional integer ambiguity resolution algorithm is obtained using multiple frequencies. The PN code is added to eliminate most of the integer ambiguity, and thus, the approach can be adapt for very long baseline ambiguity resolution.

For baselines of 3100km (11000km), and signals in the X-band the simulation results show accuracy values of 1.61 nrad (0.45nrad). Compared to other techniques at same distance, like SBI from Table1, measurement accuracy is on the same level. However, it is less limited than SBI and does not require multiple spacecraft in the same beam.

## APPENDIX

See Figures 10–13.

## REFERENCES

[1] W. R. Ren, G. L. Dong, and H. T. Li, *Engineering and Technology of Deep Space TT&C System*. Beijing, China: Science Press, 2013, pp. 87–124.
[2] J. B. Berner, S. H. Bryant, and P. W. Kinman, "Range measurement as practiced in the deep space network," *Proc. IEEE*, vol. 95, no. 11, pp. 2202–2214, Nov. 2007.
[3] L. Iess, M. Di Benedetto, N. James, M. Mercolino, L. Simone, and P. Tortora, "Astra: Interdisciplinary study on enhancement of the end-to-end accuracy for spacecraft tracking techniques," *Acta Astronautica*, vol. 94, no. 2, pp. 699–707, Feb. 2014. [Online]. Available: www.researchgate.net
[4] H. Zhou, D. Xu, S. Chen, H. Li, and G. Dong, "New high-accuracy spacecraft VLBI tracking using high data-rate signal: A demonstration with Chang'E-3," *Sci. China Technol. Sci.*, vol. 59, no. 4, pp. 558–564, Apr. 2016.
[5] J. L. Massey, G. Boscagli, and E. Vassallo, "Regenerative pseudo-noise (PN) ranging sequences for deep-space missions," *Int. J. Satell. Commun. Netw.*, vol. 25, no. 3, pp. 285–304, May 2007.
[6] A. Hellerschmied, L. McCallum, J. McCallum, J. Sun, J. Böhm, and J. Cao, "Observing APOD with the AuScope VLBI array," *Sensors*, vol. 18, no. 5, p. 1587, 1587.
[7] T. Schüler, G. Kronschnabl, C. Plötz, A. Neidhardt, A. Bertarini, S. Bernhart, L. L. Porta, S. Halsig and A. Nothnagel, "Initial results obtained with the first TWIN VLBI radio telescope at the geodetic observatory Wettzell," *Sensors*, vol. 15, no. 8, pp. 18767–18800, 2015.
[8] C. B. Haskins, D. J. Duven, C. C. DeBoy, and J. R. Jensen, "First deep-space flight demonstration of regenerative pseudo-noise ranging," in *Proc. IEEE Aerosp. Conf.*, Big Sky, MT, USA, Mar. 2012, pp. 1–6.
[9] M. Kumar, R. Agarwal, R. Bhutani, and C. Shakher, "Measurement of strain distribution in cortical bone around miniscrew implants used for orthodontic anchorage using digital speckle pattern interferometry," *Opt. Eng.*, vol. 55, no. 5, May 2016, Art. no. 054101.

[10] M. Kumar and C. Shakher, "Measurement of temperature and temperature distribution in gaseous flames by digital speckle pattern shearing interferometry using holographic optical element," *Opt. Lasers Eng.*, vol. 73, pp. 33–39, Oct. 2015.
[11] G. Pedrini, W. Osten, and M. E. Gusev, "High-speed digital holographic interferometry for vibration measurement," *Appl. Opt.*, vol. 45, no. 15, p. 3456, May 2006.
[12] C. Pérez-López, M. H. D. L. Torre-Ibarra, and F. M. Santoyo, "Very high speed cw digital holographic interferometry," *Opt. Express*, vol. 14, no. 21, p. 9709, Oct. 2006.
[13] V. Cazac, A. Meshalkin, E. Achimova, V. Abashkin, V. Katkovnik, I. Shevkunov, D. Claus, and G. Pedrini, "Surface relief and refractive index gratings patterned in chalcogenide glasses and studied by off-axis digital holography," *Appl. Opt.*, vol. 57, no. 3, p. 507, Jan. 2018.
[14] W. An and T. E. Carlsson, "Speckle interferometry for measurement of continuous deformations," *Opt. Lasers Eng.*, vol. 40, nos. 5–6, pp. 529–541, Nov. 2003.
[15] M. Roberto, M. Trevor, and A. Ricard, "The common receiver architecture for ESA radio science and delta-DOR support," *ESA Bull. Eur. Space Agency.*, vol. 128, pp. 68–74, Nov. 2006.
[16] N. James, R. Abello, M. Lanucara, M. Mercolino, and R. Maddè, "Implementation of an ESA delta-DOR capability," *Acta Astronautica*, vol. 64, nos. 11–12, pp. 1041–1049, Jun. 2009.
[17] E. Wei, W. Yan, S. Jin, J. Wei, H. Kutoglu, X. Li, J. Adam, S. Frey, and J. Liu, "Contribution of simulated space VLBI to the Chang'E-1 orbit determination and EOPs estimation," *Aerosp. Sci. Technol.*, vol. 46, pp. 256–263, Oct. 2015.
[18] G. C. Cardarilli, L. D. Nunzio, and R. Fazzolari, "Hardware prototyping and validation of a W-ΔDOR digital signal processor," *Appl. Sci.*, vol. 9, no. 14, p. 2909, Jul. 2019.
[19] K. Fuyuhiko, L. Qinghui, and M. Koji, "Simulation analysis of differential phase delay estimation by same beam VLBI method," in *Proc. 1st Selene Working Team Meeting Location*, Tsukuba, Japan: Tsukuba Space Center, vol. 60, no. 4, Jan. 2007. pp. 391–406.
[20] M. Gregnanin, B. Bertotti, M. Chersich, M. Fermi, L. Iess, L. Simone, P. Tortora, and J. G. Williams, "Same beam interferometry as a tool for the investigation of the lunar interior," *Planet. Space Sci.*, vol. 74, no. 1, pp. 194–201, Dec. 2012.
[21] C. Edwards, Jr., D. Rogstad, L. White, and D. Fort, "The goldstone real-time connected element interferometer," in *Proc. Telecommun. Data Acquisiton Prog. Rep.*, CA, USA, Aug. 1992, pp. 52–62.
[22] A. E. E. Rogers, "Very long baseline interferometry with large effective bandwidth for phase-delay measurements," *Radio Sci.*, vol. 5, no. 10, pp. 1239–1247, Oct. 1970.
[23] J. Taylor, *Deep Space Communications*. California, CA, USA: Jet Propulsion Laboratory California Institute of Technology, 2016, pp. 15–37. [Online]. Available: http://ieeexplore.ieee.org
[24] C. Lue, P. Jinsong, L. Wenxiao, and H. Songtao, "Juno radio open loop measurement experiment based on China's deep space stations," *J. Deep Space Explor.*, vol. 5, no. 4, pp. 382–386, 2019.
[25] A. R. Whitney, R. Cappallo, W. Aldrich, B. Anderson, A. Bos, J. Casse, J. Goodman, S. Parsley, S. Pogrebenko, R. Schilizzi, and D. Smythe, "Mark 4 VLBI correlator: Architecture and algorithms," *Radio Sci.*, vol. 39, no. 1, pp. 1–24, Feb. 2004.
[26] K.-M. Cheung, D. Divsalar, and S. Bryant, "Two-way ranging and Doppler for multiple orbiting spacecraft at Mars," in *Proc. IEEE Aerosp. Conf.*, Big Sky, MT, USA, Mar. 2018, pp. 1–17.
[27] E. Venosa, C. Alakija, F. Harris, and X. Chen, "How to implement deep-space regenerative pseudo-noise (PN) ranging transceivers," in *Proc. IEEE Aerosp. Conf.*, Big Sky, MT, USA, Mar. 2016, pp. 1–10.
[28] J. Yang, Y. Yang, J. Li, H. Li, and T. Yang, "A novel satellite-equipped receiver for autonomous monitoring of GNSS navigation signal quality," *Sci. China Technol. Sci.*, vol. 59, no. 7, pp. 1137–1146, Jul. 2016.
[29] X. Gang, *Principles of GPS and Receiver Design*. Beijing, China: Publishing House of Electronics Industry, 2009, pp. 359–420.
[30] J. Yang, Y. Yang, J. Li, H. Li, and T. Yang, "Analysis of noncommensurate sampling effects on the performance of PN code tracking loops," *Sci. China Technol. Sci.*, vol. 61, no. 6, pp. 893–905, Jun. 2018.
[31] A. Asef-Vaziri and M. Goetschalckx, "Dual track and segmented single track bidirectional loop guide path layout for AGV systems," *Eur. J. Oper. Res.*, vol. 186. no. 3, pp. 972–989, May 2008.
[32] C. Wei, "A robust algorithm research and design for ambiguity resolution and angle measurement in lunar rendezvous radar interferometry," M.S. thesis, School Aeronaut. Astronaut., Univ. Electron. Sci. Technol. China, Chengdu, China, 2014.
[33] Z. J. Towfic, T. J. Voss, M. M. Shihabi, and J. S. Border, "X-band PN delta DOR signal design and implementation on the JPL iris transponder," in *Proc. IEEE Aerosp. Conf.*, Big Sky, MT, USA, Mar. 2019, pp. 1–7.
[34] H. He, J. Li, Y. Yang, J. Xu, H. Guo, and A. Wang, "Performance assessment of single- and dual-frequency BeiDou/GPS single-epoch kinematic positioning," *GPS Solutions*, vol. 18, no. 3, pp. 393–403, Jul. 2014.
[35] P. Bolla and K. Borre, "Performance analysis of dual-frequency receiver using combinations of GPS L1, L5, and L2 civil signals," *J. Geodesy*, vol. 93, no. 3, pp. 437–447, Mar. 2019.
[36] G. Jianghui and B. Yehuda, "Triple-frequency GPS precise point positioning with rapid ambiguity resolution," *J. Geodesy*, vol. 88, no. 1, pp. 95–97, Jan. 2014.
[37] L. Weitao, X. Jiangfeng, H. Songtao, and C. Lue, "Construction of regional tropospheric delay model in deep space station and its application in Chang'E-4 mission," *Scientia Sinica Technologica*, vol. 11, pp. 1286–1294, Nov. 2019.
[38] X. Ju, Z. Xu, and J. Li, "The problems discussion about applications of GPS to engineering control surveying," *J. Inst. Surveying Mapping*, vol. 20, no. 1, pp. 14–17, 2003.

**LINSHAN XUE** received the B.S. degree from the University of Electronic Science and Technology of China, in 2012, where he is currently pursuing the Ph.D. degree with the School of mechanical and Electrical Engineering. His current research interests include GNSS navigation, deep space exploration, and VLBI.

**WEIREN WU** is currently a member of the Chinese Academy of Engineering and the International Academy of Astronautics, and the Chief Designer of the Chinese Lunar Exploration Project. His research interests include telemetry track and command (TT&C) and deep space exploration engineering system design.

**XUE LI** received the Ph.D. degree from Beihang University, China, in 2008. She began to work in the Chongqing University, in 2019. Her current research interests include space information power networks, GNSS navigation and deep space exploration.